Figure 8 represents the measured and simulated S_{11} of the proposed PCMA. There are some differences between the two which may be due to the effect of SMA and because of misalignment of two substrate layers. Measured S_{11} is below −10 dB over the 2.4–2.48, 3.44–3.53, 3.8-4.2, 4.74–6 GHz bands. The radiation patterns are observed in a semi-anechoic chamber. The measured 2D radiation patterns for yz-plane and xz-plane at 2.44, 3.5, 3.8, and 5.5 GHz are shown in Figure 9 and 10, respectively. The radiation patterns show broadside radiation characteristics with less cross polarization (near −15 dB). The simulated gains are 3.47/1.62/0.72/6.22 dBi at 2.44/3.5/3.8/5.5 GHz, respectively. The measured gains are 3.32/1.25/0.58/6.16 dBi at 2.44/3.5/3.8/5.5 GHz, respectively.

5 | CONCLUSION

A novel and simple multi-band proximity coupled V-slotted rectangular patch with parasitic element for wireless applications such as WiFi, WiMAX, and WLAN, and so on. is proposed. The proposed structure consists of a V-slot loaded patch with a parasitic element proximity coupled by an L-shaped microstrip line feed resulting multiple impedance bandwidths (2.4–2.48, 3.44–3.53, 3.8–4.2, 4.74–6 GHz). The proposed PCMA has potential to be used in wireless communications due to its small size and broadside radiation characteristics.

ORCID

Jayanta Ghosh http://orcid.org/0000-0002-1321-5380

REFERENCES

[1] Maci S, Gentili GB, Piazzesi P, Salvador C. Dual-band slot loaded patch antenna. *IEE Proc Microw Antennas Propagat.* 1995;142(3):225–232.

[2] Roy JS, Ghosh J. A multifrequency microstrip antenna. *Microw Opt Technol Lett.* 2005;46(1):63–65.

[3] Lee KF, Yang SLS, Kishk AA, Luk KM. The versatile U slot patch antenna. *IEEE Antennas Propagat Mag.* 2010;52(1):71–88.

[4] Mok WC, Wong SH, Luk KM, Lee KF. Single-layer single patch dual-band and triple-band patch antennas. *IEEE Trans Antennas Propagat.* 2013;61(8):4341–4344.

[5] Chakraborty U, Kundu A, Chowdhury S, Bhattacharjee A. Compact dual-band microstrip antenna for IEEE 802.11 a WLAN application. *IEEE Antennas Wirel Propagat Lett.* 2014;13:407–410.

[6] Kale GM, Labade RP, Pawase RS. Open rectangular ring slot loaded rectangular microstrip antenna for dual frequency operation. *Microw Opt Technol Lett.* 2015;57(10):2448–2452.

[7] Singh V, Mishra B, Narayan Tripathi P, Singh R. A compact quad-band microstrip antenna for S and C-band applications. *Microw Opt Technol Lett.* 2016;58(6):1365–1369.

[8] Varma R, Ghosh J, Bhattacharya R. A compact dual frequency double U-slot rectangular microstrip patch antenna for WiFi/WiMAX. *Microw Opt Technol Lett.* 2017;59(9):2174–2179.

[9] Bakariya PS, Dwari S, Sarkar M, Mandal MK. Proximity coupled multiband microstrip antenna for wireless applications. *IEEE Antennas Wirel Propagat Lett.* 2015;14:646–649.

[10] Mak C, Luk K, Lee K. Proximity-coupled U-slot patch antenna. *Electron Lett.* 1998;34(8):715–716.

[11] Lau K, Luk K, Lee K. Wideband U-slot microstrip patch antenna array. *IEE Proc Microw Antennas Propagat.* 2001;148(1):41–44.

[12] Kidder C, Li M-y, Chang K. Broad-band U-slot patch antenna with a proximity-coupled double π-shaped feed line for arrays. *IEEE Antennas Wirel Propagat Lett.* 2002;1:2–4.

[13] Ooi B-L. A double-π-stub proximity feed U-slot patch antenna. *IEEE Trans Antennas Propagat.* 2004;52(9):2491–2496.

[14] Qu S-W, Xue Q. A Y-shaped stub proximity coupled V-slot microstrip patch antenna. *IEEE Antennas Wirel Propagat Lett.* 2007;6:40–42.

[15] Wang H, Huang X, Fang D, Han G. A microstrip antenna array formed by microstrip line fed tooth-like-slot patches. *IEEE Trans Antennas Propagat.* 2007;55(4):1210–1214.

[16] Zhou Y, Chen C-C, Volakis JL. Dual band proximity-fed stacked patch antenna for tri-band GPS applications. *IEEE Trans Antennas Propagat.* 2007;55(1):220–223.

[17] Veysi M, Kamyab M, Jafargholi A. Single-feed dual-band dual linearly-polarized proximity-coupled patch antenna. *IEEE Antennas Propagat Mag.* 2011;53(1):90–96.

[18] Bakariya PS, Dwari S, Sarkar M, Mandal MK. Proximity coupled microstrip antenna for bluetooth, WIMAX, and WLAN applications. *IEEE Antennas Wirel Propagat Lett.* 2015;14:755–758.

How to cite this article: Varma R, Ghosh J. Multi-band proximity coupled microstrip antenna for wireless applications. *Microw Opt Technol Lett* 2018;60:424–428. https://doi.org/10.1002/mop.30985

Received: 13 July 2017

DOI: 10.1002/mop.30979

Dual wide-band miniaturized negative group delay circuit using open circuit stubs

Hany Taher | **Ronan Farrell**

Electronic Engineering Department, Institute of Technology Carlow-Ireland, Maynooth, Co. Kildare, Ireland

Correspondence
Hany Taher, Umm Elqura University-Faculty of engineering, Electrical Engineering, Alabdia-Makkaj, Makkah 5555, Saudi Arabia.
Email: hany.abdelrahman@nuim.ie

Funding information
Science Foundation Ireland (SFI), Grant/Award Number: 13/RC/2077

Abstract

In this letter, dual band negative group delay circuit (DBNGDC) utilizing a couple of one quarter guided wave length ($\lambda_g/4$) open circuited stubs (OCSs) is presented. The centre frequencies ($f_{01,2}$) are fully controlled with the stub lengths. On the other hand, the target negative group delay (NGD) is obtained using couple of resistors ($R_{1,2}$) that connect each OCS to the main microstrip line. The designed DBNGDC accomplishes 52% size diminution compared with smallest size has ever been achieved before. Moreover, 0.2 and 0.4 GHz zero-NGD bandwidths (BW) are achieved.

KEYWORDS

artificial neural networks (ANN), microstrip circuits, negative group delay circuit (NGDC), open circuit stubs

1 | INTRODUCTION

With the rapid development of modern wireless technologies, dual-band devices have been more and more attractive in global system for mobile communications (GSM), wireless code-division multiple-access (WCDMA), world-wide interoperability for microwave access (WiMax), and especially in the newly developed wireless local area networks (WLANs) standards.

On the other hand, negative group velocity, and consequently NGD, is an example of abnormal wave propagation phenomena and it could be observed within the limited frequency band of signal in certain media under signal attenuation condition.[1] This phenomenon is exploited to build NGDCs which are required in diverse applications and systems such as efficiency enhancement of feedforward linearization,[2] beam-squit minimization in phased array antenna systems,[3] and eliminating phase variation with frequency in phase shifters.[4]

There are considerable works provide many techniques to design a single band NGDC. As example, microstrip defected ground structure (DGS) technique which is adopted in Ref. [5] and negative dielectric permittivity stopband microstrip Lines which is utilized in Ref. [6]. On the other hand, there are just few papers evolve efficient designs for DBNGDC. A composite right/left handed (CRLH) transmission line is presented in Ref. [7]. Even though, it has narrow bandwidth large area size and complicated design procedure. The attenuation characteristic of the defected microstrip structure (DMS) and are harnessed to overcome the aforementioned disadvantage.[8] However, in this letter, only one couple of $\lambda_g/4$ OCSs is utilized to realize simpler design, smaller size, and wider bands DBNGDC.

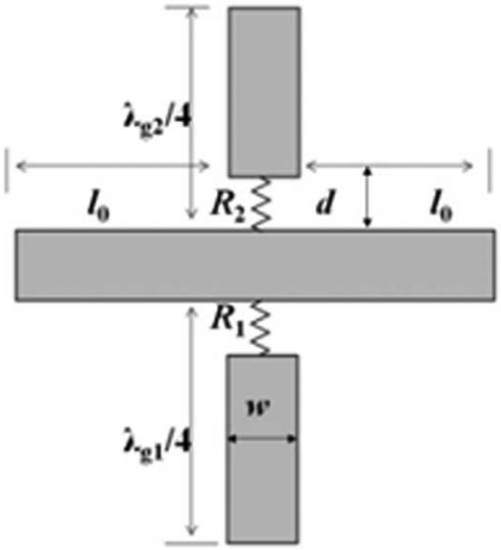

FIGURE 1 The proposed DBNGDC

This letter is organized as follows. The theory of the presented DBNGDC is presented in Section 2. In Section 3, implementation of the design procedure and verification of the proposed methodology with measurements is elaborated. Conclusions will be drawn in Section 4.

2 | PROPOSED DBNGDC UNIT

The proposed DBNGDC is shown in Figure 1. Two OCSs are connected to the main microstrip line via two resistors R_1 and R_2, respectively. The OCSs and the main line have 50 Ω characteristic impedance (Z_0) and consequently all have the same width (w). On the other hand, the OCSs have lengths (measured from the main line) amount to $\lambda_{g1}/4$ and $\lambda_{g2}/4$, where λ_{g1} and λ_{g2} are the guided wavelengths at f_{01} and f_{02}, consecutively.

On the other hand, the input and output ports lengths (l_0) are fixed to 10 mm. Moreover, the distance from the main line to each OCS (d) is fixed to 0.2 mm. The utilized substrate in all simulations and in the fabrication stage is RT/Duroid 5880 with a dielectric constant of 2.2 and thickness of 0.79 mm. All the simulations are carried out using time-domain finite integration technique implemented in CST microwave studio package.

Each OCS resonates at predetermined specific frequency due to its specific length. As example, at finite frequency range around the resonance frequency, f_{01}, the signal is maximally attenuated and NGD phenomenon is occurred. The equivalent circuit of the DBNGDC, at f_{01}, is shown in Figure 2. Concerning the OCS under resonance, it is modeled as a lossless shunt-connected series combination of a capacitance

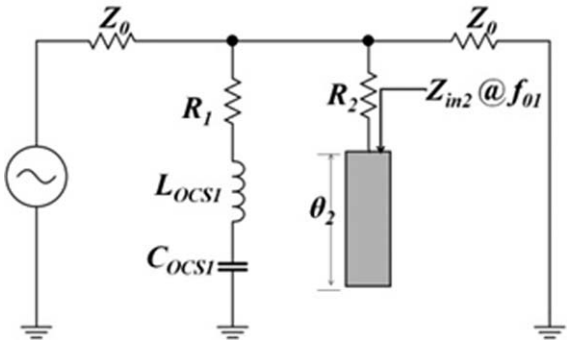

FIGURE 2 Equivalent circuit of DBNGDC at f_{01}

and an inductance. Furthermore, the resonator is added to the R_1 that connects it to the main line. On the other hand, the second OCS has finite input impedance (Z_{in2}) in series with R_2 and all are in parallel with the series resonator of the first OCS. Moreover, it has an electrical length (θ_2) at f_{01}. The same analysis is valid at the second resonance, f_{02}, by mutually replace one with two and vice versa at the subscript of the relevant quantities in the aforementioned discussion.

Accordingly, $f_{01,2}$ are completely and independently determined using the resonator lengths, $\lambda_{g1,2}$, which are determined using the following relation,

$$\lambda_{g1,2}=\frac{\lambda_{01,2}}{\sqrt{\frac{\varepsilon_r+1}{2}+\frac{\varepsilon_r-1}{2}\frac{1}{\sqrt{1+12\frac{h}{w}}}}} \tag{1}$$

where, $\lambda_{01,2}$ are the free space wave length at f_{01} and f_{02} consecutively, furthermore, ε_r and h are the dielectric constant and the thickness of the used substrate, respectively.

On the other side, $\tau_{1,2}$ are calculated from the equivalent circuit of the proposed structure, as follows,

$$\tau_{1,2}=-\frac{1}{2\pi}\frac{d\angle S_{21}}{df}\Big|_{f_{01,2}} \tag{2}$$

From the DBNGDC equivalent circuit, the values of $\tau_{1,2}$ are influenced by parameters of the two OCSs concurrently. The value of $\tau_{1,2}$ are highly dependent on $\theta_{2,1}$, as well as, R_1 and R_2. As an example, this dependency could be formulated, for τ_1, as follows:

$$\tau_{1,2}=f_{1,2}\left(R_1,\ \theta_{2,1},\ R_2\right) \tag{3}$$

where, $f_{1,2}$ are complicated functions and have three independent variables. However, as $\theta_{1,2}$ are determined beforehand to specify the target frequencies, that is, they are 90° at the required frequencies. Therefore, $\tau_{1,2}$ could be expressed as function of R_1, R_2 as follows:

$$\tau_{1,2}=g_{1,2}(R_1,R_2) \tag{4}$$

For the design purpose, the following function is sought,

$$(R_1,R_2)=h(\tau_1,\tau_2) \tag{5}$$

Consequently, to design DBNGDC, first, Equation 1 is utilized to obtain the OCSs lengths, and then, h is built to compute the needed R_1 and R_2 which should be harnessed to get the targeted τ_1 and τ_2. In this work, ANN is employed to acquire h.

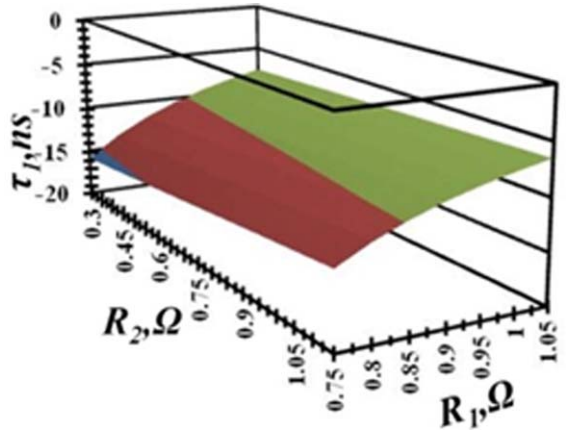

FIGURE 3 Dependency of τ_1 on R_1 and R_2 for the proposed DBNGDC [Color figure can be viewed at wileyonlinelibrary.com]

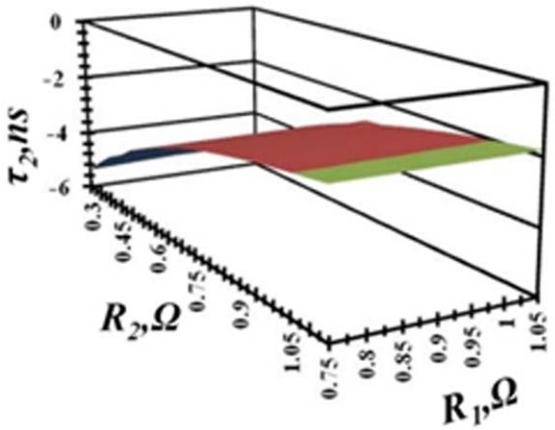

FIGURE 4 Dependency of τ_2 on $R1$ and $R2$ for the proposed DBNGDC [Color figure can be viewed at wileyonlinelibrary.com]

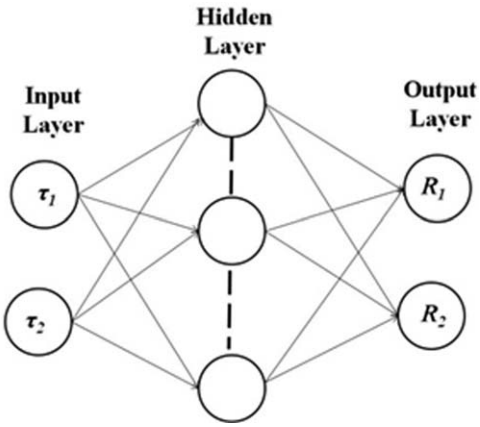

FIGURE 5 Schematic of the ANN used to design DBNGDC

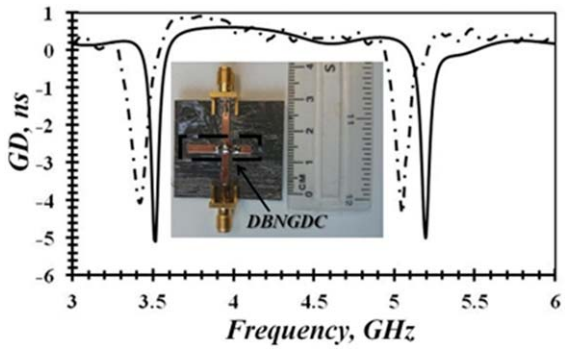

FIGURE 6 Fabricated DBNGDC accompanied by the simulation results, solid line, and the measurement results, dotted-dashed line of group delay [Color figure can be viewed at wileyonlinelibrary.com]

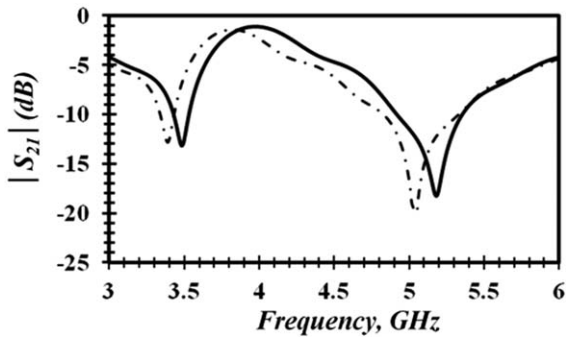

FIGURE 7 Simulation results, solid line, and the measurement results, dotted-dashed line of the transmission coefficient of DMNGDC

3 | DBNGDC DESIN AND IMPLEMENTATION

The goal is to design a DBNGDC for WiMax and WLAN operating at $f_{01,2}$ of 3.5 and 5.2 GHz, respectively. The calculated $\lambda_{g1}/4$ and $\lambda_{g2}/4$ are 15.5 and 10.5 mm, respectively and are kept to these values meanwhile the remaining part of the work. Many designs, 150 designs, with different combinations of R_1 and R_2 are simulated and the corresponding $\tau_1$and τ_2 are listed.

This data set is employed for two purposes, firstly, to build ANN model as it will be shown later. The second is to parametrically study the circuit, that is, investigate the impact of the R_1 and R_2 on τ_1 and τ_2. As depicted in Figure 3. Clearly, τ_1 is decreased as R_1 increases, whereas, R_2 alterations do not lead to a tangible effect. The same behavior is still noticed for the other side, that is, for τ_2, as it is shown in Figure 4. It is obvious that the variations of R_1 have small impact on τ_2 values, while, increasing R_2 lowers τ_2 values.

Multilayer perceptrons (MLP) is the most popular structure of ANN models. It follows a general class of structure called feedforward ANN. Moreover, they have a capability of the general approximation of any nonlinear function.[9] The input neurons of the built ANN are τ_1 and τ_2, while, its outputs neurons are R_1 and R_2, respectively, as shown in Figure 5. The number of hidden layer neurons is 21. Besides, the training error as well as the test one is $<1.75\%$.

The established ANN is now used to design the aimed OCSs DBNGDC. With inputs of -5 ns, the obtained values of R_1 and R_2 are 1.3 and 0.3 Ω, respectively. The designed circuit is fabricated using printed circuit board (PCB) technology, and measured utilizing vector network analyzer (VNA), photocopy of the fabricated circuit is shown in Figure 6. Comparison between simulation and measurement results for DNGDC is shown in Figure 6. There is little discrepancy between the predicted locations and values of the NGD quantity and their realized counterparts.

The reason of the location inconsistency is due to what so-called edge effect of the OCSs, where, the electromagnetic field pattern of the OCS does not vanish abruptly at the end of the stub. Therefore, this phenomenon adds a parasitic capacitance to the end of the OCS. As a consequence, it could be modeled as an additional length added to the physical length of the line, resulting in the effective length being slightly longer than the physical one, and as a result, the measured resonance frequency gets lower than the simulated counterpart. Concerning the NGD values discrepancy, it is attributed to inevitable fabrication uncertainties due to the limited available laboratory equipments.

On the other side, good agreement between simulation and measurements results of transmission coefficient is noticed as depicted in Figure 7.

Table 1 shows the performance comparison of the proposed circuit with the previous research results. Concerning the area size, the smallest DBNGDC area have ever been accomplished, was published in Ref. [8] and it amounts to

TABLE 1 Performance comparison of the proposed DBNGDC with other works

	Frequency (GHz)		NGD (ns)		Band width (MHz)			
	f_{01}	f_{02}	f_{01}	f_{02}	f_{01}	f_{02}	Area (λ_{01}^2)	No. of stages
[7]	2.14	3.50	−3	−3.1	180	180	1 × 0.5	2
[8]	3.50	5.20	−4.5	−4.2	275	240	0.046 × 0.5	2
This work	3.50	5.20	−5	−5	200	400	0.028 × 0.4	1

45×4 mm^2. However, the proposed OCSs based DBNGDC occupies only 48% from this value, as depicted in Figure 4 inside the dotted box. Moreover the proposed DBNGDC exhibits the overall highest BW value among the other works. Take into account that it is only single stage, not two, as the other previous designs. Therefore, the demonstrated unit is superior in both of size and frequency behavior aspects. Consequently and unequivocally the demonstrated DBNGDC has the best overall performance among the others.

4 | CONCLUSION

In this letter, miniaturized DBNGDC using pair of $(\lambda_g/4)$ OCSs is developed. Due to the attenuation characteristic of OCS, the NGD phenomenon is occurred at the allocated frequency. On the other hand, utilizing external resistor allow us to control NGD values. ANN is built and exploited to design the developed DBNGDC. Furthermore, the designed DBNGDC is fabricated and verified experimentally. Compared to the previously published results, the proposed DBNGDC has the smallest size and the widest BW. It is expected that the presented DBNGDC would help to minimize the area size of contemporary wireless communication systems.

ORCID

Hany Taher http://orcid.org/0000-0001-6875-3381

REFERENCES

[1] Mojahedi M, Malloy KJ, Eleftheriades GV, Woodley J, Chiao RY. Abnormal wave propagation in passive media. *IEEE J Select Topic Quant Electron.* 2003;9(1):30–39.

[2] Choi H, Jeong Y, Kim CD, Kenney JS. Efficiency enhancement of feedforward amplifiers by employing a negative group delay circuit. *IEEE Trans Microw Theory Tech.* 2010;58:1116–1125.

[3] Oh SS, Shafai L. Compensated circuit with characteristics of lossless double negative materials and its application to array antennas. *IET Microw Antennas Propag.* 2007;1:29–38.

[4] Ravelo B, Roy ML, Perennec A. Application of negative group delay active circuits to the design of broadband and constant phase shifters. *Microw Opt Tech Lett.* 2008;50(12):3078–3080.

[5] Chaudhary G, Jeong J, Kim P, Jeong Y, Lim J. Compact negative group delay circuit using defected ground structure," in Proc. of Asia-Pacific Microwave Conference, 2013, 22–24.

[6] Taher H, Farrell R. Highly miniaturized wideband negative Group delay circuit using effective negative dielectric permittivity stopband microstrip lines, in Proc. of 46th European Microwave Conference (EuMC), 2016, 112–115.

[7] Choi H, Jeong Y, Lim J, Eom SY, Jung YB. A novel design for a dual-band negative group delay circuit. *IEEE Microw Wireless Compon Lett.* 2011;21(1):19–21.

[8] Chaudhary G, Jeong Y, Lim J. Miniaturized dual-band negative group delay circuit using dual-plane defected structures. *IEEE Microw Wireless Compon Lett.* 2014;24(8):521–523.

[9] Scarselli F, Tsoi AC. Universal approximation using feedforward neural networks: a survey of some exciting methods, and some new results. *Neural Networks.* 1998;11(1):15–37.

How to cite this article: Taher H, Farrell R. Dual wide-band miniaturized negative group delay circuit using open circuit stubs. *Microw Opt Technol Lett* 2018;60:428–432. https://doi.org/10.1002/mop.30979

Received: 18 July 2017

DOI: 10.1002/mop.30984

Compact dual band slotted triangular monopole antenna for RFID applications

M. Dehmas | A. Azrar | F Mouhouche | K. Djafri | M. Challal

Institute of Electrical and Electronic Engineering, Laboratory of Signal and Systems, University M'hamed Bougara, Boumerdes, Algeria

Correspondence
Azrar Arab, Institute of Electrical and Electronic Engineering, University of Boumerdes, Boumerdes, Algeria.
Email: a.azrar@univ-boumerdes.dz

Abstract

This paper presents a compact monopole antenna for radio frequency identification (RFID) systems. The proposed antenna is a dual band structure that can operate in the frequency ranges [0.797–1.004 GHz] and [2.234–2.934 GHz]. Consequently, the antenna covers widely the two UHF bands dedicated for RFID applications which are [0.860–0.960 GHz] and [2.380–2.520 GHz]. Moreover, the antenna is compact and its wide band nature makes it suitable for several applications other than RFID (GSM, UMTS, Wi-Fi, Bluetooth, etc.). The proposed antenna has been fabricated and its reflection coefficient measured where a good agreement is observed with the simulated results.

KEYWORDS

compact microstrip antenna, dual band, RFID, slotted triangular monopole